Preprint typeset in JHEP style. - HYPER VERSION

arXiv:astro-ph/0001084 6 Jan 2000

Signatures of galactic magnetic lensing upon ultra high energy cosmic rays

Diego Harari[a], **Silvia Mollerach**[b] **and Esteban Roulet**[b]

[a] *Departamento de Física, FCEyN, Universidad de Buenos Aires*
Ciudad Universitaria - Pab. 1, 1428, Buenos Aires, Argentina
[b] *Departamento de Física, Universidad Nacional de La Plata*
CC67, 1900, La Plata, Argentina
Email: harari@df.uba.ar, mollerac@venus.fisica.unlp.edu.ar, roulet@venus.fisica.unlp.edu.ar

ABSTRACT: We analyse several implications of lensing by the regular component of the galactic magnetic field upon the observed properties of ultra high energy cosmic rays. Magnetic fields deflect cosmic ray trajectories, causing flux (de)magnification, formation of multiple images of a single source, and time delays. We derive the energy dependence of these effects near the caustics at which the flux amplification of a point source diverges. We show that the large magnification of images around caustics leads to an amplification bias, which can make them dominate the flux in some energy ranges. We argue that clustering in the arrival directions of UHECRs of comparable energy may be due to magnetic lensing around caustics. We show that magnetic lensing can also significantly alter the observed composition of cosmic rays at the highest energies. We also show that the time delay between events from a single image may monotonically decrease with decreasing energy in the neighborhood of a caustic, opposite to its behaviour in normal regions.

KEYWORDS: High-energy cosmic rays.

Contents

1. Introduction 1

2. Flux enhancement by magnetic lensing near critical points 2

3. Angular distribution of events: clustering around caustics 6

4. Effects upon composition 9

5. Time delays 10

6. Conclusions 12

A. Magnification near caustics 14

B. Magnification for two nearby folds 15

1. Introduction

Galactic and intergalactic magnetic fields deflect extragalactic charged cosmic ray trajectories in their journey from their sources to the Earth, causing several effects upon the observed properties of ultra high energy cosmic rays (UHECRs). For a review see for instance [1].

In a previous paper [2] (in what follows paper I), we have shown that the regular component of the galactic magnetic field acts as a giant lens upon charged CRs, and this can sizeably amplify (or demagnify) the flux arriving from any given source, modifying its spectrum. The magnification of the CR flux by the galactic magnetic field becomes divergent for directions along critical curves in the sky seen from the Earth, corresponding to caustic curves in the "source plane", i.e. in the corresponding directions outside the Galaxy. The location of the caustics move with energy and, as a caustic crosses a given source direction, pairs of additional images of the source appear or disappear. Multiple image formation is a rather common phenomenon, at least within the galactic magnetic field models considered in I. Indeed, the caustics sweep a rather significant fraction of the sky as the ratio E/Z between the CR energy and charge steps down to values of the order of a few EeV (1 EeV = 10^{18} eV), before the drift and diffusive regimes turn on. At values of E/Z larger than around 50 EeV

caustics are present but sweep out a relatively small fraction of the sky. The effects under discussion are thus relevant even for the highest energy events so far detected if the CRs have a component which is not light.

In the present paper we analyse in detail the energy dependence of the magnification of image pairs near a caustic, and discuss several implications of the existence of caustics upon the observed properties of UHECRs.

In section 2 and in appendix A we show that if a source lies along a caustic at energy E_0, the magnification factor μ of each image in the pair that becomes visible at energies below E_0 diverges as $\mu \approx A/\sqrt{1-E/E_0}$. A is a dimensionless constant, fixed by the structure of the magnetic field along the CR trajectory to the source. It must be determined numerically, and we do so for some examples of source locations. We discuss several implications of this result, such as the expected enhancement in the observed event rate at energies near a caustic, which can lead to an amplification bias, making it more likely to detect images of UHECR sources that lie along caustics than sources in ordinary regions. In appendix B we provide a simple proof of the relation between the magnification of the three images appearing when there are two nearby folds. In section 3 we show that the angular separation between images in a pair increases near the caustic as $\Delta\theta \propto \sqrt{1-E/E_0}$. We analyse the expected event rate from the original source and its multiple images not only as a function of energy but also in terms of the observed arrival direction. We show that magnetic lensing near caustics is a source of clustering in the arrival directions of events with comparable energy. In section 4 we stress the fact that at fixed energy the magnetic lensing effects depend upon the CR electric charge, and show that this dependence can significantly alter the observed CR composition at the highest energies. In section 5 we discuss features of the time delay between events from multiple images, relevant in the case of bursting or highly variable sources of UHECRs [3]. We show that the delay between the arrival of events of equal energy from the two images in a pair increases as $\Delta t \propto \sqrt{1-E/E_0}$ around a caustic. We also show that the time delay between events at different energy from one image in a pair may monotonically decrease with decreasing energy near the caustic, opposite to the behaviour of time delays in normal regions. Section 6 rounds up our conclusions.

The galactic magnetic field model that will be used throughout this paper to illustrate magnetic lensing effects is the bisymmetric spiral model with even symmetry (BSS-S) described in paper I, which is a smoothed version of one of the models used in [4] and [5] to study the effects of CR deflections in our galaxy. We refer the reader to paper I for details about the field configuration and about the numerical methods implemented to determine CR trajectories and flux magnifications.

2. Flux enhancement by magnetic lensing near critical points

As shown in paper I, the galactic magnetic field can act as a giant lens that amplifies

or demagnifies extragalactic sources of UHECRs, much alike the gravitational lensing effect upon distant quasars by intervening matter along the line of sight [6]. CRs from a distant extragalactic source that enter the galactic halo from a direction $(\ell, b)_H$ (in galactic coordinates) are deflected by the magnetic field and thus observed on Earth as if coming from a different direction $(\ell, b)_E$, and their flux is amplified (or demagnified) by a factor μ. The magnitude of the effect depends upon the direction of observation and upon the ratio E/Z between energy and charge of the CR. The effect is most dramatic at the critical curves of the lens mapping, the directions along which the observed flux diverges for a fixed value of E/Z. The corresponding lines in the source coordinates (the direction from which CRs enter the galactic halo) are the caustics of the lens mapping. The location of the caustics changes with energy, for fixed Z.

If a source position lies along a caustic of the magnetic lens mapping at energy E_0, a pair of images of the source either becomes visible or dissapears at energies below E_0. Their magnification diverges at $E = E_0$. This behaviour was illustrated in paper I for sources at galactic coordinates $(\ell, b) = (282.5°, 74.4°)$ (M87 in the Virgo cluster) and $(\ell, b) = (320°, -30°)$ (visible from the southern hemisphere).

In appendix A we give a geometrical interpretation of the magnification of a pair of images near a caustic. Similar to the gravitational lens case [7, 8, 9], the magnification diverges as $1/\sqrt{x}$, where x measures the distance of the source to the caustic. In the magnetic lensing case the location of the caustics "move" with energy, and thus the magnification of a pair of images diverges as the energy approaches the energy at which the source lies along the caustic as $1/\sqrt{E_0 - E}$. In appendix A we also find the first two corrections to this leading order behaviour, and show that the magnification of the two images behaves as:

$$\mu_i(E) \approx \frac{A}{\sqrt{1 - E/E_0}} \pm B + C_i \sqrt{1 - E/E_0} \ . \tag{2.1}$$

The dimensionless coefficient A is the same for the two images. The constant term $\pm B$ has the same value with opposite sign for each image. The third term has a different coefficient C_i for each image due to the truncation of the expansion up to this order. The value of the coefficients A, B and C_i are fixed by the properties of the magnetic field along the CR trajectories. We determine them through a fit to the numerical output for the energy dependence of the amplification, evaluated through the method described in paper I.

Figure 2 displays the numerical result for the amplification near the caustics along with the fit to the analytic expression in eq. (2.1), for the same examples of source locations as in paper I. The top panel corresponds to M87 and the bottom panel to the source in the southern hemisphere. The figures display the magnification of the principal image (the one that is also visible at the highest energies) and of the images A and B, visible at energies below the caustic only. The analytic expression

(2.1) fits with very high accuracy the numerical result for the magnification of the secondary images near the caustic, at least down to energies 10% below the energy E_0 of the caustic. The fit to M87 determines $E_0/Z = 20.41$ EeV, $A = 1.3$, $B = 4.0$, $C_A = -3.1$, $C_B = 5.0$. The fit to the southern source fixes $E_0/Z = 15.425$ EeV, $A = 0.44$, $B = 0.37$, $C_A = -0.19$, $C_B = -0.28$.

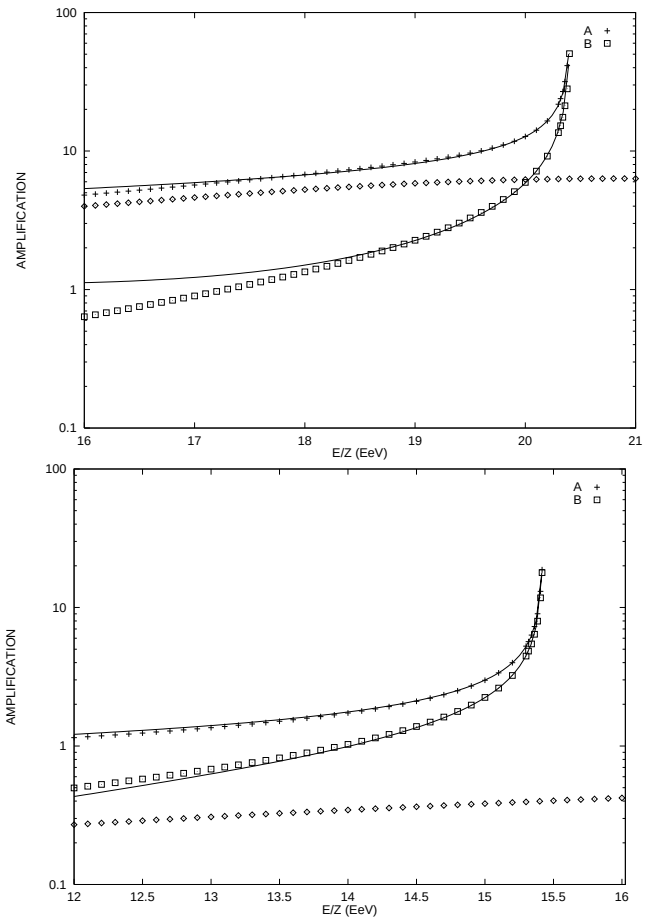

Figure 1: Numerical result (points) and analytic fit to eq. (2.1) (solid lines) for the amplification near a caustic of a pair of images of a point source. The source in the top panel is at $(\ell, b) = (282.5°, 74.4°)$ (M87) and the source in the bottom panel is at $(\ell, b) = (320°, -30°)$. The numerical result for the amplification of each principal image (diamonds) is also shown.

The divergence of the flux magnification of a CR source at $E = E_0$ is softened down to finite values when integrated across an extended source. This still allows for extremely large magnifications. The limiting factor to the maximum attainable magnification in a realistic situation is not the extended nature of the sources, but the fact that the divergence in the magnification, even in the case of a point source, arises only at a fixed energy E_0. Since realistic sources are not monoenergetic, the integrated flux of a magnified source around E_0 is thus always finite, even in the point source approximation.

Large magnification of image pairs around caustics leads to a significant enhancement of the detection probability of a source in a flux-limited sample. In gravitational lensing this effect is termed "amplification bias"[10], and may be responsible for the observation of quasars that would otherwise be too dim to detect. Let us now consider the strength of this effect due to galactic magnetic lensing of UHECRs. Consider a differential flux of CRs injected in the galactic halo at energies beyond the "ankle" given by $dF = F_0(E_0/E)^{2.7}dE$. The flux observed on Earth coming from two images formed at a caustic at energy E_0, in the energy interval between 0.9 E_0 and E_0, is

$$F_{A+B}(0.9E_0 < E < E_0) \approx 2\int_{0.9E_0}^{E_0} \mathrm{d}E \frac{\mathrm{d}F}{\mathrm{d}E}\frac{A}{\sqrt{1-E/E_0}} \approx 12A\int_{0.9E_0}^{E_0} \mathrm{d}E \frac{\mathrm{d}F}{\mathrm{d}E}\ . \quad (2.2)$$

We have neglected a small $O(\sqrt{1-E/E_0})$ correction (the term proportional to $C_A + C_B$). The flux observed from the two images in this energy interval near the caustic is $12A$ times larger than the flux of the principal image of the source in the same energy range in the absence of magnification. This is also $2.4A$ times the flux that would arrive from the principal image at all energies above E_0 if there were no magnetic lensing. Detection of an UHECR source in a narrow energy range around a caustic may thus be more likely than its detection at any higher energy. It may also be more likely to detect the CR source at energies around the caustic than at significantly lower energies (say half the energy of the caustic or even less) in cases where both the principal image as well as the secondary images are not magnified at energies below the caustic.

Large enhancements of the observed flux in a narrow energy range also occur in the interesting case when the source position lies along two caustics at nearby energies so that the principal image of the source (the only one visible from Earth at the highest energies) has also divergent magnification. Such a situation is exemplified in figure 2, for a source located at $(\ell = 90°, b = -10°)$. A pair of images becomes visible at energies below $E_0^{III} = 29.31$ EeV, one of which disappears in a caustic along with the principal image at an energy $E_0^I = 22.31$ EeV. The secondary image that merges with the principal image is that with opposite parity.

In appendix B we develop the geometrical interpretation and analytic approximation to the magnification of images for two nearby folds. The analog result in the gravitational lens case was obtained in [9]. As shown in appendix B, and verified numerically with high accuracy, between the folds the sum of the magnifications of the two images with equal parity coincides with the magnification of the image with opposite parity, up to a constant term. The analytic fits in figure 2 to the divergent magnification of the principal image (I) at E_0^I and to the magnification at E_0^{III} of the image that survives at low energies (III), lead to $A_I = 0.275$, $B_I = 0.15$, $C_I = 0.63$; $A_{III} = .096$, $B_{III} = -0.11$, $C_{III} = 0.03$. The magnification of the image that is visible at energies between E_0^I and E_0^{II} is fit to $\mu_{II} = \mu_I + \mu_{III} - 0.7$.

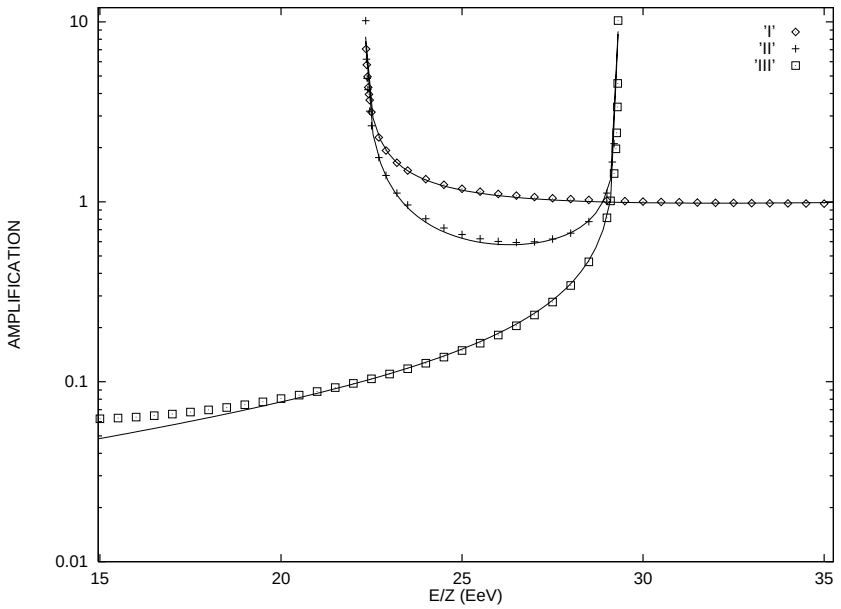

Figure 2: Example of a source position that is crossed by two folds at nearby energies. The solid lines for images I and III are the analytic fits of the numerical results to eq. (2.1) for the amplification near a caustic. The solid line for image II is $\mu_I + \mu_{III} - 0.7$. The source is located at $(\ell, b) = (90^\circ, -10^\circ)$.

3. Angular distribution of events: clustering around caustics

The arrival directions of the so far detected CRs in the highest energy range is compatible (within the limited statistics available) with an isotropic distribution, except for some small angle clustering of events (eight doublets and two triplets within a total of 92 events with energies above 40 EeV)[11]. The observed relatively uniform distribution does not preclude the possibility that UHECRs originate from very few nearby sources, if their trajectories underwent significant energy-dependent deflections in their journey to the Earth. Trajectories of UHECRs with E/Z below approximately 50 EeV are sensibly deflected in the magnetic field model considered in this paper. Several quite separated events may actually originate from the same source if CRs have a component which is not light (see paper I and references therein). It has even been speculated [12] that all the events so far detected at energies above 10^{20} eV may come from M87 in the Virgo cluster, if the Galaxy has a rather strong and extended magnetic wind.

In paper I we illustrated the angular displacement in the arrival directions of CRs from the principal and secondary images of a magnetically lensed source. Here we analyse in more detail the angular displacement of image pairs around caustics. We argue that caustics can produce a significant clustering of arrival directions of events with comparable energies.

It may well be the case (depending on the sources flux and composition, and on

the exact nature of the galactic magnetic field) that a large fraction of the trajectories of the UHECRs so far detected have been significantly bent and do not point to their sources. In this scenario clustering of events would be infrequent, at relatively low energies due to large deflections and at high energies due to the smaller flux. However, when a source is near a caustic, since the significant enhancement of its flux occurs within a narrow energy range, the CRs arrive from relatively nearby directions, leading to an angular concentration of events.

We illustrate the clustering effect in figure 3. We consider the same examples of source locations as in the previous section. We assume that the differential flux injected by the source scales as $E^{-2.7}$, and that the detecting system has the same efficiency at all energies within the range considered. The energy range was divided in 50 bins of equal detection probability. Figure 3 displays the predicted arrival directions of the events detected from each source.

In the case of M87 (top panel) 11 events out of a total of 50 with E/Z larger than 10 EeV (half the energy of the caustic) fall in the narrow energy range between the energy of the caustic and just 10% below ('+' signs). 3 of those 11 events are in the principal image and 8 in the secondary images. Notice that only 5% of the events would fall in the same energy range if the source were not magnified. Notice also that just 8 events correspond to the principal image at all energies higher than the energy of the caustic. The angular clustering effect for M87 is significant but not extremely large (in this magnetic field model), partly due to the fact that the principal image is also largely magnified around the energy of the caustic, and partly because deflections are quite large.

The middle panel in figure 3 displays the effect for the source located at $(\ell, b) = (320^\circ, -30^\circ)$. In this case 9 events fall within 10% of the energy of the caustic in the secondary images, separated by no more than 5°. Only 4 events are seen for all energies higher than the energy of the caustic, scattered over almost 10°. The events at energies below the caustic, down to half its energy, are scattered over more than 20°.

The bottom panel in figure 3 corresponds to the source located at $(\ell, b) = (90^\circ, -10^\circ)$, which presents two nearby folds, as depicted in figure 2. In this case nearly half of the events (23) fall within the energy range between the two caustics (22.3 EeV $< E/Z <$ 29.3 EeV), while 15 events occur for all higher energies, and just 12 events appear at lower energies down to $E/Z = 7$ EeV. The relatively small number of events in the lower energy range is due to the large deamplification of the image flux. An unlensed source would have instead 86% of the events in the lower energy range considered, 9% in the higher energy range, and just 5% at the intermediate energies. Notice that while the arrival directions of the events considered are spread over more than 15°, nearly half of the events fall within just 2° around $(l = 88^\circ, b = -11^\circ)$.

We stress the fact that six out of the eight doublets in the UHECR data listed

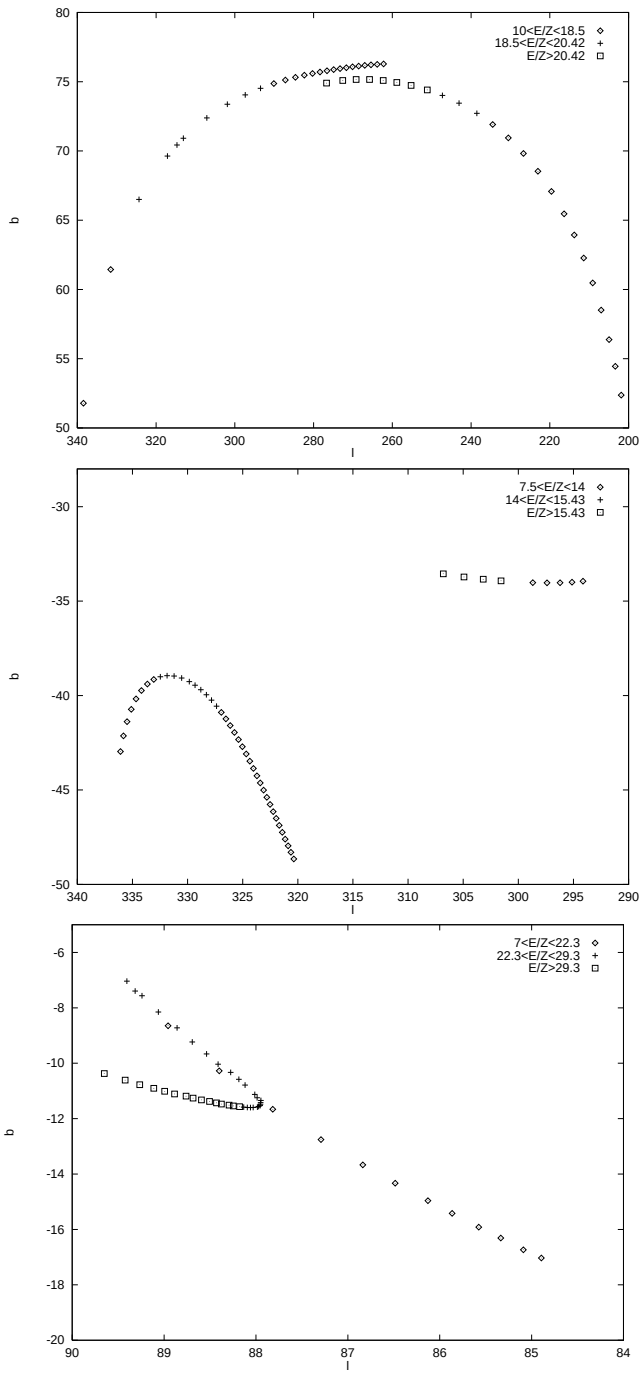

Figure 3: Predicted arrival directions of 50 UHECR events from M87 (top) and from the sources at $(\ell, b) = (320^\circ, -30^\circ)$ (middle) and $(\ell, b) = (90^\circ, -10^\circ)$ (bottom), that illustrate the clustering effect due to the existence of caustics in the magnetic lens mapping.

in table 6 in [11] are such that the energies of the events in a pair differ by less than 10%. The same happens with two events in one of the triplets. This may be an indication that at least a fraction of the observed clustering of events may be due to magnetic lensing around caustics.

Figure 3 (and figure 6 in paper I) illustrate the angular displacement of the images as a function of energy. As discussed in appendix A, the observed angular separation between images scales as $\sqrt{x}$, where x measures the distance from the source to the caustic. Consequently, the angular separation between the pair of images created at the caustic crossing scales with energy near a caustic as

$$\Delta\theta \approx \Theta\sqrt{1 - E/E_0}\ . \tag{3.1}$$

The proportionality constant Θ is fitted from the numerical output for the angular displacement of the images. In the case of M87, $\Theta \approx 56°$, and in the case of the source at $(\ell, b) = (320°, -20°)$ it is $\Theta \approx 15.1°$.

4. Effects upon composition

Another interesting effect of magnetic lensing is that it can strongly alter the measured composition of CRs at high energies. This is because at each source location the magnification is a function of E/Z. Thus, for a given energy the CR flux of components with different Z suffers different (de)magnification as the CRs travel through the Galactic magnetic field.

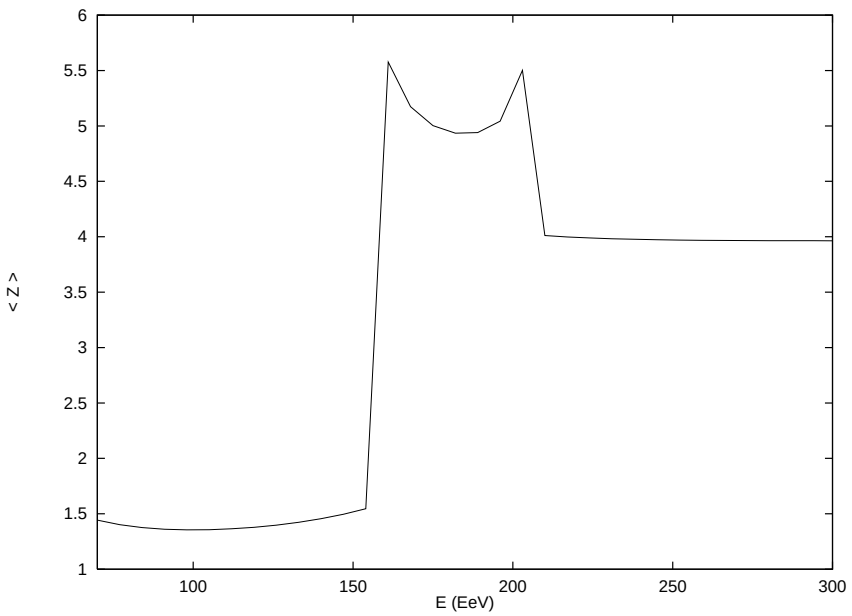

Figure 4: Illustration of the effect of magnetic lensing upon the UHECR observed composition. The source is located at $(\ell, b) = (90°, -10°)$, and undergoes the magnification depicted in figure 2. The source injects 50% of protons and 50% of Nitrogen. In the absence of lensing the mean value of Z would be $\langle Z \rangle = 4$, independently of energy.

To give an idea of the strength of this effect, let us consider a simple example: suppose that from a given source the CR flux arriving to the halo is composed by a

fraction f of protons and a fraction $1-f$ of heavier nuclei with charge Z_h. In the absence of magnetic lensing the mean value of Z of the arriving particles would be $\langle Z\rangle = f + (1-f)Z_h$. Due to the effect of the magnetic field, the flux of protons on Earth will be (de)magnified by $\mu(E)$ and the flux of heavier nuclei by $\mu(E/Z)$. Thus, the mean value of Z of the CRs arriving on Earth will be

$$\langle Z\rangle = \frac{f\mu(E) + (1-f)Z_h\mu(E/Z_h)}{f\mu(E) + (1-f)\mu(E/Z_h)}. \tag{4.1}$$

As the magnifications can be large, $\langle Z\rangle$ can be strongly modified by the magnetic field. The effect is specially important for regions of the sky for which the total magnification μ (adding the contribution from all the images) has noticeable changes as E/Z varies.

We show as an example the source located at $(\ell, b) = (90°, -10°)$, which undergoes the magnification depicted in figure 2. We took for reference a flux composed by a fraction $f = 0.5$ of protons and a fraction 0.5 of Nitrogen ($Z_h = 7$). In the absence of lensing the mean value of Z would be $\langle Z\rangle = 4$. We see in figure 4 that a clear change from a light composition in the smaller energy region to a heavier composition at the larger energies appears due to magnetic lensing.

5. Time delays

A charged UHECR that traverses a distance L within a homogeneous magnetic field B perpendicular to its trajectory is deflected by an angle of the order of $\eta \simeq 5°(10\ \mathrm{EeV}\ Z/E)(B/\mu\mathrm{G})(L/\mathrm{kpc})$, in the limit of small deflections. Consider two initially parallel CRs emitted simultaneously, one with a much lower ratio E/Z than the other. If they enter a region permeated by a homogeneous magnetic field and converge to the same point after a distance L, the CR with lower ratio E/Z arrives later, with a relative time delay $\delta t \approx \eta^2 L/2 \approx 10\ \mathrm{yrs}(10\ \mathrm{EeV}\ Z/E)^2(B/\mu\mathrm{G})^2(L/\ \mathrm{kpc})^3$. Higher energy events arrive earlier.

Time delays induced by intergalactic magnetic fields are an essential ingredient in bursting models for the origin of UHECRs [3]. There are very definite observational signatures of such a scenario. For instance, individual bursting CR sources would have very narrow observed spectra, since only CRs with a fixed time delay would be observed at any given time. The energy at the peak in the differential CR flux received on Earth should shift with time as $t^{-1/2}$.

Here we analyse the implications of the regular component of the galactic magnetic field upon time delays between events from a UHECR source at different energies, and between events from different images of a single magnetically lensed source.

Since UHECRs are extremely relativistic, their time delay compared to straight propagation at the speed of light from the source to the observer is simply determined by the excess path length. We assume that the extragalactic UHECR sources are

sufficiently distant that we can approximate the CR flux incident upon the galactic halo as a beam of parallel trajectories, all emitted simultaneously. We then numerically determine the difference in path length between the trajectory of a charged CR and the path length along the parallel straight trajectory in the beam that reaches the Earth. In other words, we measure the delay in the arrival time of a charged CR with respect to the arrival time of photons (or charged CRs with much higher energy) emitted simultaneously from a distant source.

Figure 5 displays the time delay with respect to straight propagation for the principal and secondary images of the source locations discussed in the previous sections.

The time delay in normal regions (far from critical points) monotonically increases with decreasing energy. The spiraled galactic magnetic field is far from homogeneous, and thus departures from the E^{-2} dependence are certainly expected. We have checked that the time delay averaged over a regular grid of arrival directions scales, in the BSS-S galactic magnetic field model considered, as $< \delta t > \approx$ 1000 yrs(10 EeV $Z/E)^2$ from very high energies down to E/Z of order 5 EeV. At lower E/Z values the increase in the time delay with decreasing energy is faster, since a sharp transition from quasirectilinear to drift motion occurs at values of E/Z between 3 and 1 EeV.

What strikes the eye in figure 5 is that the time delay of one of the images in a pair can have an energy dependence opposite to that in normal regions. Indeed, the time delay of one of the images that are visible at energies below the energy of the caustic increases with decreasing energy, while the time delay of the other member of the pair decreases. Thus, the relative arrival time of events from a single image of a CR source does not necessarily increase with decreasing energy. It is often argued that the doublets in which the highest energy event arrived later than the other member in the pair can not arise from bursting sources. As we have seen, this is not necessarily true near a caustic.

The relative arrival time delay between equal energy events from different images A and B in a pair behaves near the caustic as

$$\Delta t = \delta t_A - \delta t_B \approx T\sqrt{1 - E/E_0}\ . \tag{5.1}$$

This can be understood as follows, in the limit of small deflections. The trajectory of each of the images in the pair is deflected by η and $\eta + \Delta\theta$ respectively, with $\Delta\theta$ given by eq. (3.1). The time delays with respect to straight propagation are thus proportional to η^2 and $\eta^2 + 2\eta\Delta\theta$ respectively, as long as $\Delta\theta \ll \eta$. Thus the relative time delay between events at the same energy from the two images scales as $\Delta\theta$ at energies sufficiently close to that of the caustic. The fit of eq. (5.1) to the numerical output is highly accurate, with $T \approx 3200$ yrs in the case of M87 and $T \approx 1030$ yrs in the case of the source in the southern sky at $(\ell = 320°, b = -30°)$.

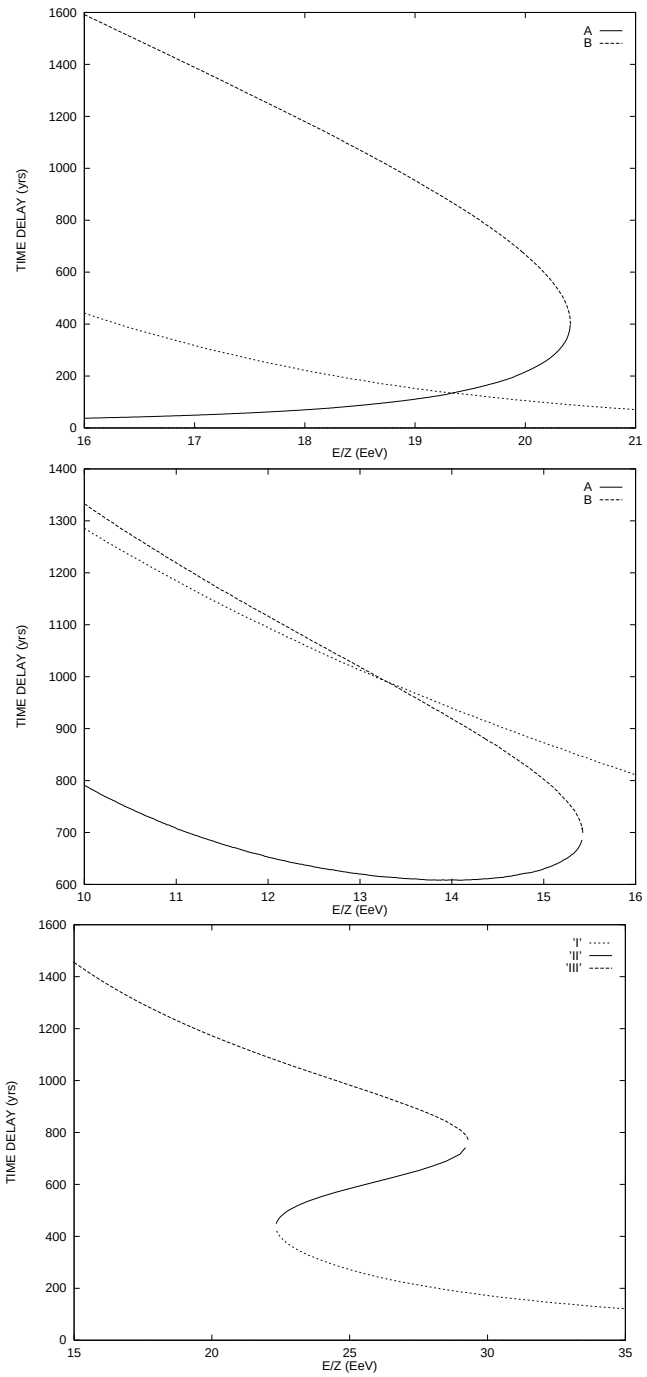

Figure 5: Time delays in the arrival of UHECRs from the principal and secondary images a distant source, measured with respect to the arrival time of a photon (or a much more energetic charged CR). The relative arrival time delay of a pair of images near the caustic scales as $\delta t \propto \sqrt{1 - E/E_0}$. Notice that the arrival time of one of the images **decreases** for decreasing E below the energy caustic, opposite to the behaviour in normal regions.

6. Conclusions

UHECRs beyond the ankle in the spectrum are most probably nuclei of extragalactic

origin. In their way to the Earth they feel the magnetic field structure permeating the Galaxy and hence their trajectories become deflected and their fluxes are lensed. The implications of this magnetic lensing are manyfold and they have to be taken into account in the analysis of the observations.

Since the lensing effect depends on the energy it can sizeably affect the observed spectrum of the sources. Moreover, for sources located in a large fraction of the sky CRs can reach the Earth following different paths, and hence multiple images of those sources will appear. A useful way to visualise these effects is to display the mapping of the arrival directions in the Earth into the incoming directions outside the Galaxy, as was introduced in paper I with what was dubbed a 'sky sheet'. In the locations where this surface develops folds, pairs of additional images of the source are present. These folds, corresponding to the caustics, move with energy, and as they cross a given source location pairs of additional images appear or disappear. Near the fold the magnification of each image in the pair diverges as $\mu \propto 1/\sqrt{|E - E_0|}$. Thus the probability to detect events from a given source is noticeably enhanced for energies close to E_0, at which the caustic crosses the source location. This also leads to an expected concentration of events near the location at which the new pair of images appears. This is relevant in the analysis of the small scale clustering present in the UHECR distribution and in this respect it is remarkable that the observed events in doublets and triplets in most cases are very close in energies. With the increased statistics expected with the new detectors, such as Auger [13] or High Res [14], these features may become testable through a careful analysis of the clustering of the events.

Also the observed CR composition can be affected by magnetic lensing due to the dependence of the flux amplification on E/Z. Nuclei with different charges are magnified by different amounts for a given energy. This effect is sizeable for sources whose magnification has a strong energy dependence (in particular when there are caustics) and which have a mixed composition.

Another feature which we have discussed is the time delay due to the galactic field between the different images of a lensed source. These are typically larger than the lifetimes of the CR observatories, and are strongly dependent on the energy. If burst sources exist, narrow spectra will then result at any given time, and the different images will be observed simultaneously with different E/Z values.

We have to stress that in addition to the effects related to the magnetic field of the Galaxy discussed in this paper there may be also similar effects associated to the magnetic field in the source galaxy or even to the intergalactic fields if these ones are strong. Also the magnetic field model adopted here is plausible but the real one may differ from it, changing the quantitative details but not the general qualitative results.

Acknowledgments

Work partially supported by ANPCyT, CONICET and Fundación Antorchas, Argentina.

A. Magnification near caustics

The relation between the source position and the image positions is given by a mapping from the source coordinates $(\ell, b)_H$ to the observer's ones $(\ell, b)_E$. When this mapping is multiple valued there will be additional image pairs appearing (see paper I). The magnification of a given image will be $\mu = \mathrm{d}\Omega_H/\mathrm{d}\Omega_E$, i.e. the ratio of differential solid angles associated to the mapping.

To visualise these facts it is useful to consider the inverse map $(\ell, b)_E \to (\ell, b)_H$ and look at it as the mapping of a surface (the observer's sky) into another surface (dubbed the 'sky sheet' in I), which will be folded when multiple images appear, and whose stretching is related to the magnification of the images. The location of the folds correspond to the caustics along which image pairs with divergent magnification appear and the magnification varies very rapidly with the distance to the fold. Since the folds move as the energy is decreased, the knowledge of the magnification as a function of the angular distance to the fold for a given energy can be used to obtain the magnification, for a given source, as a function of the energy near a caustic, which is the quantity of interest to us here.

The angular dependence of the magnification near a fold has a very simple geometrical interpretation in terms of the folded sky sheet. Let us take local angular coordinates (x, y) in the source sky such that $x = 0$ describes locally the location of the fold (and hence the fold is along the y axis while the x axis is orthogonal to it). We can also adopt (non–orthogonal) local coordinates on Earth (X, Y) such that $X = 0$ is mapped into $x = 0$ and similarly $Y = 0$ is mapped into $y = 0$. Furthermore, we will assign a third coordinate to the mapping, i.e. $(X, Y) \to (x, y, z)$, giving a depth to the sky sheet so that the fold can be visualised. The simplest choice for this (arbitrary) third coordinate is to take $z = X$, as we will do in the following. The results will be easier to obtain with this choice, but are independent of it. In this way the mapping for a fixed value of Y in a neighbourhood of $X = 0$ will look as shown in figure 6. The magnification is given by $\mu = |K\mathrm{d}X/\mathrm{d}x|$, where $K \equiv [\cos b_H |\partial(\ell, b)_H/\partial(x, y)|]/[\cos b_E |\partial(\ell, b)_E/\partial(X, Y)|]\mathrm{d}y/\mathrm{d}Y \simeq K_0(Y) + K_1(Y)X + O(X^2)$. The next step is to relate the factor $\mathrm{d}X/\mathrm{d}x = \mathrm{d}z/\mathrm{d}x$ with the slope of the curve in figure 6, and approximate the fold near the caustic by its Taylor expansion $x = az^2 + bz^3 + O(z^4)$. Hence we have

$$\frac{\mathrm{d}x}{\mathrm{d}z} \simeq 2az + 3bz^2 \tag{A.1}$$

and hence, since $z = \pm\sqrt{x/a}(1 + O(x))$, with the sign indicating to which side of the fold the image belongs, we have

$$\mu = \frac{A'}{\sqrt{x}} \pm B' + O(\sqrt{x}), \tag{A.2}$$

A' and B' being x-independent parameters related to the parameters a, b, K_0 and K_1.

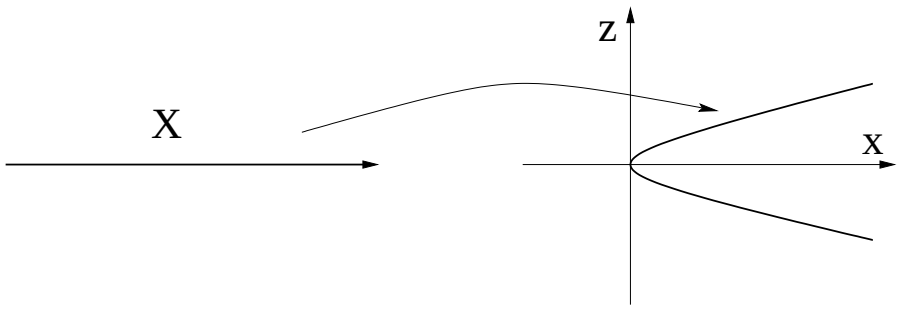

Figure 6: Mapping from the observer's sky (X) into the source sky (x), for fixed Y, with the vertical coordinate ($z = X$) allowing to visualise the fold in the sky-sheet.

The final step is to relate this with the magnification for one given source as a function of energy. Suppose that at energy E_0 a source located at $(\ell_0, b_0)_H$ would be just on top of the fold. If we define the angular 'velocity' of the fold as the energy is changed as $V(E) \equiv \mathrm{d}x_f/\mathrm{d}E$, with x_f being the distance from the source to the fold ($x_f = 0$ for $E = E_0$), one has $x_f \simeq V(E_0)|E_0 - E|$. Hence we finally get

$$\mu(E) = \frac{A}{\sqrt{1 - E/E_0}} \pm B + O(\sqrt{1 - E/E_0}). \tag{A.3}$$

B. Magnification for two nearby folds

The previous Appendix dealt with the magnification for the two images which appear when a fold crosses the source location. The third image (e.g. the one present originally) was assumed to be far from the fold so that its magnification was supposed to have a non-singular behaviour. Another situation of interest is when two folds are nearby (e.g. when the sky–sheet has a narrow fold which moves with energy across the source, rather than becoming wider and remaining on top of the source, or when the source is near a cusp where two folds merge) so that the three images can have large magnifications.

When a couple of nearby folds crosses a source, we see that a pair of images appear at some energy and at a somewhat smaller energy one of the new images merges with the original one present at high energies and they disappear (figure 2). In this case there is a relation between the magnification of the three images, as we now show. A similar relation holds in the gravitational lens case [9].

Following similar lines as in the previous Appendix, the folded surface can be described as in figure 7. Without loss of generality we can choose the origin $x = 0$ so that the vertical coordinates of the other two images at z_1 and z_2 in figure B satisfy $z_2 = -z_1$. In this case a Taylor expansion of the fold will be $x = az^3 - cz$ (with $a, c > 0$ and no quadratic term due to our choice of origin for x). The location of the folds are at $x_I = -2a(c/3a)^{3/2}$ and $x_{II} = -x_I$. The images in region I ($z > z_I = \sqrt{c/3a}$) and III ($z < z_{II} = -z_I$) will have positive parities, while the one in region II ($z_{II} < z < z_I$) will have negative parity.

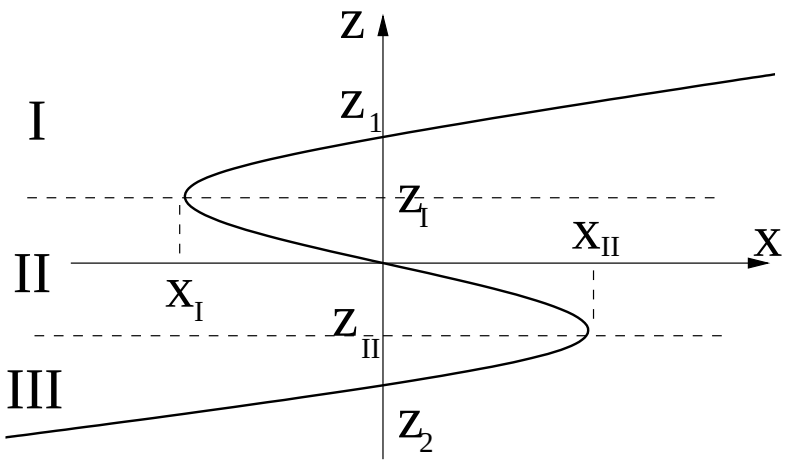

Figure 7: Sky-sheet in the source sky corresponding to two nearby folds (for Y fixed).

The vertical coordinates of the three images for a given x are simply obtained as

$$z_k = 2z_I \cos\frac{\alpha + 2k\pi}{3} \qquad (k = 0, 1, 2) \tag{B.1}$$

where $\cos\alpha = x/x_{II}$. Here $k = 2$ corresponds to the negative parity image (region II) while $k = 0$ and 1 are the images in region I and III respectively.

The magnification of the images will be $\mu_k = K|\mathrm{d}z_k/\mathrm{d}x|$, where

$$\frac{\mathrm{d}z_k}{\mathrm{d}x} = \frac{2z_I}{3x_{II}\sqrt{1-(x/x_{II})^2}} \sin\left[\frac{\cos^{-1}(x/x_{II})}{3} + \frac{2k\pi}{3}\right]. \tag{B.2}$$

From this we find that

$$\left|\frac{\mathrm{d}z_0}{\mathrm{d}x}\right| + \left|\frac{\mathrm{d}z_1}{\mathrm{d}x}\right| = \left|\frac{\mathrm{d}z_2}{\mathrm{d}x}\right|, \tag{B.3}$$

i.e. that the sum of the magnifications of the two positive parity images coincides with the magnification of the negative parity image.

Next to leading terms (i.e. corrections of $O(\sqrt{x})$ will add constant terms to the magnifications, so that the final result up to corrections of $O(x)$ is

$$\mu_I + \mu_{III} = \mu_{II} + \mathrm{const.} \tag{B.4}$$

This theorem is illustrated in figure 2.

References

[1] P. Bhattacharjee and G. Sigl, "Origin and propagation of extremely high-energy cosmic rays", *Phys. Rep.* (in press), `astro-ph/9811011`.

[2] D. Harari, S. Mollerach and E. Roulet, *J. High Energy Phys.* **08** (1999) 022.

[3] J. Miralda-Escudé and E. Waxman, *Astrophys. J.* **462** (1996) L59; E. Waxman and J. Miralda-Escudé, *Astrophys. J.* **472** (1996) L89.

[4] T. Stanev, *Astrophys. J.* **479** (1997) 290.

[5] G. Medina Tanco, E. De Gouveia dal Pino and J. Horvath, *Astrophys. J.* **492** (1998) 200.

[6] P. Schneider, J. Ehlers and E. E. Falco, *Gravitational Lenses*, Springer-Verlag, 1992.

[7] K. Chang and S. Refsdal, *Nature* **282** (1979) 561.

[8] R. Blandford and R. Narayan, *Astrophys. J.* **310** (1986) 568.

[9] P. Schneider and A. Weiss, *Astron. Astrophys.* **260** (1992) 1.

[10] E.L. Turner, J.P. Ostriker and J.R. Gott III, *Astrophys. J.* **284** (1984) 1.

[11] Y. Uchihori, M. Nagano, M. Takeda, M. Teshima, J. Lloyd-Evans, A.A. Watson, "Cluster analysis of extremely high energy cosmic rays in the northern sky", `astro-ph/9908193`.

[12] E.J. Ahn, G. Medina-Tanco, P. L. Biermann, T. Stanev, "The origin of the highest energy cosmic rays: do all roads lead back to Virgo?", `astro-ph/9911123`.

[13] http://www.auger.org/auger.html

[14] http://bragg.physics.adelaide.edu.au/astrophysics/HiRes.html